



LAWRENCE
LIVERMORE
NATIONAL
LABORATORY

First electron-positron pair experiments using the Osaka LFEX laser

H. Chen

October 15, 2012

New Journal of Physics

Disclaimer

This document was prepared as an account of work sponsored by an agency of the United States government. Neither the United States government nor Lawrence Livermore National Security, LLC, nor any of their employees makes any warranty, expressed or implied, or assumes any legal liability or responsibility for the accuracy, completeness, or usefulness of any information, apparatus, product, or process disclosed, or represents that its use would not infringe privately owned rights. Reference herein to any specific commercial product, process, or service by trade name, trademark, manufacturer, or otherwise does not necessarily constitute or imply its endorsement, recommendation, or favoring by the United States government or Lawrence Livermore National Security, LLC. The views and opinions of authors expressed herein do not necessarily state or reflect those of the United States government or Lawrence Livermore National Security, LLC, and shall not be used for advertising or product endorsement purposes.

First electron-positron pair experiments using the Osaka LFEX laser

Hui Chen¹, M. Nakai², Y. Sentoku³, Y. Arikawa², H. Azechi², P. Beiersdorfer¹, S. Fujioka², C. Keane¹, S. Kojima², W. Goldstein¹, B. R. Maddox¹, N. Miyanaga², T. Morita², T. Nagai², H. Nishimura², T. Ozaki², J. Park¹, Y. Sakawa², H. Takabe², G. Williams¹, Z. Zhang²

1. Lawrence Livermore National Laboratory, Livermore, California 94551, USA

2. Institute of Laser Engineering, Osaka University, 2-6 Yamadaoka, Suita, Osaka 565-0871, Japan

3. Department of Physics, University of Nevada, Reno, Nevada 89557, USA

ABSTRACT

We report the results from the first laser driven electron-positron experiment using the high power LFEX laser at the Institute of Laser Engineering at Osaka University. A number of diagnostics were set up to measure electrons, positrons, x-rays and neutrons from the laser-target interaction at the relativistic regime. Together with high-energy electrons ($T_{\text{hot}} \sim 10$ MeV), relativistic positrons (~ 10 MeV) were observed from 1 kJ shots with laser intensity of about 10^{19} W/cm² on 1 mm thick gold target. Laser-electron energy transfer was inferred from the x-ray and neutron measurements and is consistent with the electron and positron data. Electron accelerations in plasmas with density below critical were found to play an important role in producing very high energy (>20 MeV) electrons, while the number of relatively low energy electrons (~ 10 MeV) appeared to be crucial to the total number of pairs produced.

Introduction

Rapid progress in laser technology in recent years is evident in the establishments of new facilities [1] near or at petawatt (10^{15} W/cm²) power. Such facilities enable a number of physics applications to be studied including fast ignition research for inertial confined fusion experiments [2], proton generation and acceleration [3, 4], MeV photon source development [5-7], and recently, electron-positron antimatter production [8, 9]. Fast electron generation and transport from relativistic-intensity laser-target interactions is the primary driver of these applications and is the subject of a great deal of over the past decades. For example, fast electrons have been investigated using techniques such as K-alpha measurements [10-12], K-alpha imaging [13], bremsstrahlung measurements [14], nuclear activation [15] and direct measurement of escaping electrons. The diagnostic capability to observe positrons produced from laser-plasma interactions has recently been added. Positrons are most efficiently produced in thick targets by the Bethe-Heitler process [16] that begins with high-energy electrons generated from laser-target interaction. First, bremsstrahlung γ -rays are created by fast electrons scattering in the field of high-Z nuclei. An electron-positron pair is then formed from the γ -ray photon decaying in the presence of a second nucleus. Positrons, therefore, are informative to understand the physics in relativistic laser target interactions, albeit through multi-step processes.

Intense laser produced electron-positron pairs are interesting on their own right due to the fact that they are a new source of positrons applicable to a variety of research disciplines including laboratory astrophysics, basic plasma science and antimatter research and applications [9]. Understanding the characteristics of laser-produced

positrons and further optimizing their density and energy are important preparatory steps in order to realize laboratory applications in these fields.

We performed a pair creation experiment using the LFEX laser at the Institute of Laser Engineering at Osaka University. By observing electrons, positrons distribution, x-rays, and photon-neutrons simultaneously, it is possible to understand quantitatively the production processes of these high-energy particles and photons in the relativistic regime. From these measurements, we obtained the dependency of positrons on the fast electron distribution and the correlation among electrons, positrons, K-shell x-rays and neutrons.

We found that very high-energy electrons ($T_{\text{hot}} \sim 10$ MeV) were produced from the LFEX experiments, indicating a large fraction of the laser pulse interacted with the long scale length plasma at under-critical density formed by a pre-pulse or energy pedestal on the main pulse. These observations are confirmed by photon-neutron measurements as well as particle-in-cell simulations using PICLS code [17]. The inferred laser-to-electron conversion from x-ray measurement was 10% - 20%, somewhat less than that reported elsewhere [2, 10, 18]. Positrons were observed on two shots. Data comparisons show that the rates between laser energy to that of electrons at energy around 10 MeV seemed to have a larger impact to the positron production. Finally, simulations show that the peak energy location in the positron spectra reflects magnitude of the sheath potentials, a quantity critical to proton and positron acceleration, formed by the fast electrons transported through the massive target.

Experimental setup

The LFEX laser [19] has four beams, two of which were used during this experimental campaign. A laser pulse of duration 1-2 ps with a 1.053 micron wavelength was focused by an $f/10$ off-axis parabola to a focal spot of 40-50 μm , resulting in a laser intensity of $1\text{-}2 \times 10^{19} \text{ W/cm}^2$, and a laser-plasma interaction in the relativistic regime. The contrast between the laser pedestal and main pulse was about $10^6 - 10^8$, which leads to a relatively long (up to 10 μm) electron density scale length before the peak pulse arrives to the target. The shot parameters are listed in Table 1.

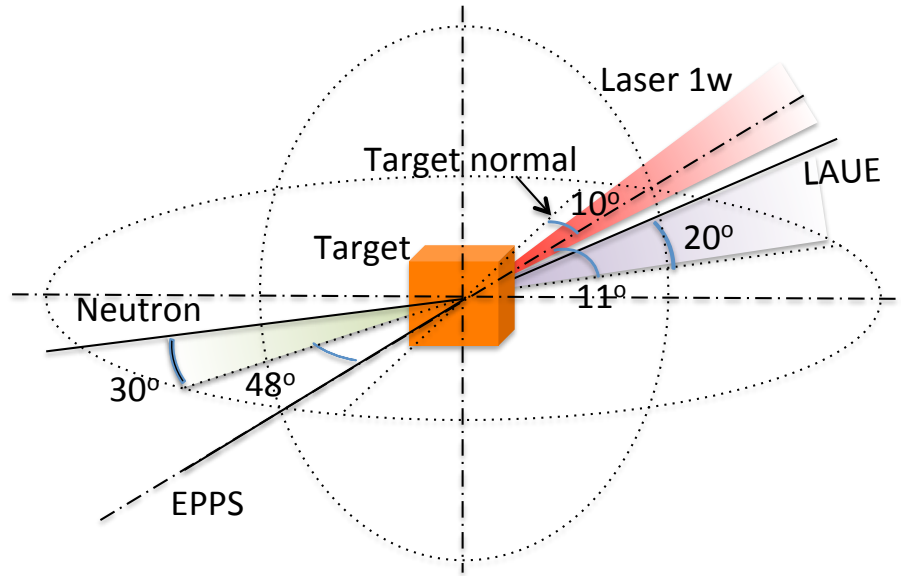


Figure 1: Diagnostic setup at LFEX laser.

The diagnostic setup relative to the incident laser and target is shown in Fig. 1. The LFEX laser was incident on the target (1 mm thick, 2 mm diameter gold discs) at 10 degree relative to the target normal direction. A Laue crystal spectrometer [20], electron-positron spectrometer EPPS [21] and neutron diagnostics [22] were placed on the opposite side of the laser. The orientations of the diagnostic line-of-sights are marked in the figure. The Laue crystal spectrometer measures the gold characteristic K-shell

radiation from which laser-electron coupling can be derived [20, 23, 24]. The EPPS electron-positron spectrometer [21] measures the energy distribution of electrons and positrons between 1-100 MeV. The neutron detectors [22] measure the number of neutrons at four energy ranges, from which the high-energy electrons and Bremsstrahlung photons can be estimated [22]. All three types of diagnostics were absolutely calibrated prior to the experiment.

Both the Laue and EPPS diagnostics use image plates as detector whose calibration was made with GE image plate scanner. In this experiment, a GE model Typhoon FLA 7000, was used. To ensure an absolute measurement could be derived from these diagnostics, we established the sensitivity calibration of this new scanner using a radiocarbon source that was cross-calibrated to a Fuji FLA 7000 scanner [21]. This process resulted in an empirical sensitivity conversion formula [25], allowing the scanner to operate at Fuji-equivalent sensitivity settings and permitting measured values to be directly compared to results from experiments on other laser facilities.

Experimental Results and Discussions

The experimental results are summarized in Table 1 for shots taken at different laser energies and intensities. The targets were identical 1 mm thick and 2 mm diameter gold disc. As comparison, data taken at Titan laser at Lawrence Livermore National Laboratory is listed for the same target and laser intensity.

The laser intensity is averaged over the focal spot. Hot electron temperatures are the derived from the EPPS measurement for electrons with kinetic energies less than

(T_{hot1}) and greater than (T_{hot2}) 10 MeV. The total number of hot electrons from EPPS is obtained by integrating the whole measured spectrum. A More detailed discussion of the electron measurement and simulation are in following section.

The laser-electron conversion efficiencies (η_e) are obtained using the Laue diagnostic measurements of gold K-alpha and K-beta lines [20] by

$$\eta_{K\alpha} \propto \frac{\eta_e}{T_{hot}} \int_0^\infty dE \sigma_{K\alpha}(E) \int_0^d dx \frac{\exp(-E/T_{hot})}{T_{hot}} \exp(-\frac{x}{\lambda_{mfp} \cos\theta}) , \quad \text{where laser transfer}$$

efficiency is η_e and the hot electron temperature is T_{hot} . The term $\exp(-\frac{x}{\lambda_{mfp} \cos\theta})$ describes the reabsorption of K_α photons during the propagation through the target material where θ is the angle between the spectrometer and target normal. Using the two-temperature (T_{hot1} and T_{hot2}) Maxwellian electron distribution measured by EPPS, an assumption of electron reflux [23], and relativistic cross-section correction, the laser-electron conversion was estimated [26]. The derived conversion efficiency is proportional to laser intensity, but somewhat less than that from the 30% - 50% reported previously [2, 10, 18].

The total number of neutron produced from the experiment is between $\sim 10^6 - 10^9$. Since these neutrons are generated primarily by photon-nuclei interaction, the shot-to-shot fluctuation of neutron yield directly correlates with the distribution of high-energy photons and consequently the high-energy electrons. This is also in qualitative agreement with the T_{hot} of each shot. Although a highly convoluted process due to the energy dependent photon-neutron cross-section feature with strong resonance features [22], one can estimate the number of high-energy gamma photons ($h\gamma$) through a simple relation

(assuming one-photon process dominates the photon-neutron process):

$$N_n \propto \int_0^\infty f(h\nu)\sigma(h\nu)d(h\nu) , \text{ where } \sigma \text{ is photon energy dependent cross section.}$$

Assuming a constant Bremsstrahlung-positron cross-section (Bethe-Heitler process [16]), the conversion efficiency from photon to positron is about 1%. Therefore we can then make a bulk prediction of positron numbers from this independent diagnostic. This is consistent (in order of magnitude) with the measured positron yield, considering about 1% of total produced positrons are measured by EPPS [27].

Table 1: Summary of experimental results. The columns are (from left to right): Shot number; On target laser energy E (in joules); Temperature of hot electrons (from EPPS, in MeV) for electrons that had kinetic energy less (T_{hot1}) and greater (T_{hot2}) than 10 MeV; Number of hot electrons from EPPS, $N(e)$, in number/sr; Laser to hot electron energy conversion efficiency, $\eta(e)$, inferred from Laue and EPPS; Number of total neutron, $N(n)$, measured from detector; Number of high energy photons, $N(\gamma)$, derived from neutron data; Measured positron number, $N(e+)$, from EPPS; Laser to EPPS positron conversion efficiency, $\eta(e+)$.

Shot	E (J)	I (W/cm ²)	T _{hot1} (MeV)	T _{hot2} (MeV)	N(e)	$\eta(e)$ %	N(n)	N(γ)	N(e+)	$\eta(e+)$ %
1	1675	1.2e19	1.8	16	8.2e11	15	2e9	8e14	2.3e10	0.003
2	1200	1e19	1.5	13	8.0e11	11	1e9	5e14	6.8e9	0.001
3	493	6e18	0.5	5	6.2e10	5	2e7	2e13	-	-
4	305	7e18	0.8	6.5	7.9e10	8	5e6	4e12	-	-
Titan	261	1.5e19	0.5	6	8.0e11	-	-	-	1.1e10	0.015

1. Electron distributions

The fast electron distribution was measured using EPPS are shown in Fig. 2. The electron spectra in Fig. 2 can be described with two distinctive temperatures for those at low energy (<10 MeV) and high energy (>10 MeV). Although EPPS measured the electrons that escaped the targets, its distribution, especially those at high energies, reflects well that produced by laser-target interaction [28, 29]. At low energy (<10 MeV)

where the electrons energies are equal or less that of the sheath potential, it is still a topic of debate as to the precise correlation of the number of escaping electrons to total number produced by lasers [28, 29]. The electron temperature T_{hot2} are much higher than that of the intensity scaling. For example, for laser intensity of $2 \times 10^{19} \text{ W/cm}^2$, the electron temperature is $\sim 1 \text{ MeV}$ according to Ponderomotive scaling [30], 0.6 MeV in Beg scaling [11] and Haines scaling [31]. It is possible that these fast electrons were accelerated from under critical density plasma by the lasers through mechanisms described by [32-34].

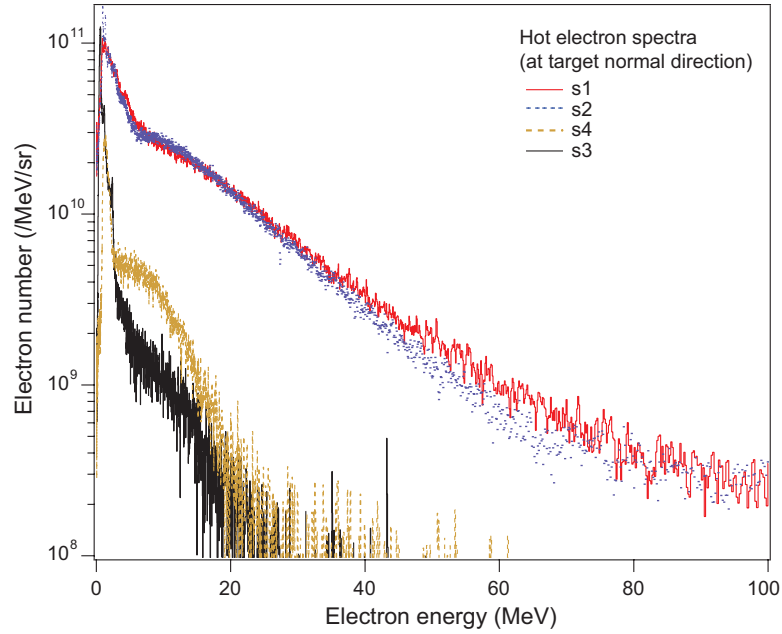


Figure 2: LFEX electron spectra measured by EPPS.

For the same laser intensity, a comparative electron spectrum observed on the Titan laser is shown in Fig. 3, showing a much cooler electron distribution from the Titan laser relative to that of LFEX. This may due to the differences in laser contract and in parabola aspect ratio ($f/3$ on Titan and $f/10$ on LFEX) in two lasers. The ratio of measured electron energy to laser energy was about $1-2 \times 10^{-3}$ on both LFEX and Titan lasers. We

can assume the ratio of escaping electrons (measured) versus the laser produced electrons remains constant for the same target [29]. We can therefore conclude that both laser systems have similar energy-to-electron conversion efficiencies. However, it should be noted that the ratio of electron number at about 10 MeV relative to the laser energy on LFEX was about 10% that of that on Titan, an important factor in understanding the positron data, as described in next section.

To better understand the LFEX data we performed one-dimensional particle-in-cell simulations using PICLS code [17] for the LFEX and Titan laser conditions. We prepared a gold target with 1mm thickness with a preplasma in front of the target. Since the LFEX has a slightly higher contrast ratio than the Titan, we initialized the simulation by placing a preplasma with a 10 μm scale length for the LFEX and a few μm scale length for the Titan. The simulation contained all relevant physics regarding the transport in the high Z gold target, including Coulomb collisions, impact ionizations, and Bremsstrahlung radiation. The laser duration was set to 2 ps for the LFEX and 700 fs for the Titan. The total simulation time was about 24 ps, which is long enough to see the electrostatic potential evolution at the target surface and the energy transport and decay in the gold target. We keep the input laser energy ratio between two pulses similar with the experiments, ~ 6 . The peak laser intensity is set to $2 \times 10^{19} \text{W/cm}^2$ for the Titan and $4 \times 10^{19} \text{W/cm}^2$ for the LFEX laser, which is higher than the experimental ones. The higher intensity compensates for one-dimensional limitations, namely, the lower absorption due to lack of multi-dimensional effects such as self-focusing and/or filamentation. Nevertheless, the purpose of these simulations is to qualitatively compare these two laser

systems on the basis of hot electron production, sheath potential created at the back surface of the gold target, and the resulting affect on the positron spectra.

Figure 3 shows the hot electron spectra observed in both experiments and simulations. Note here that the experiments see the escaping electrons and simulations show the hot electrons inside the target at the time when the pulse is done.

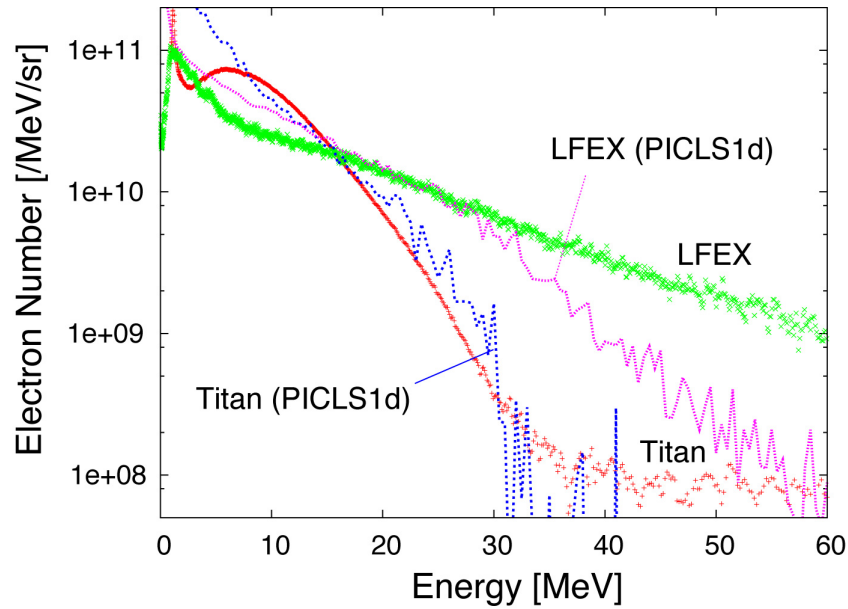


Figure 3: Comparison of electron spectrum from LFEX and Titan, and PICLS simulations.

Positron measurement

Positron data were obtained for the two high laser energy shots (#1 and #2) on the LFEX experiment, as listed in Table 1. For the two low energy shots (#3-#4), the positron signal was too weak to allow any quantitative measurement of positrons. A comparison of positron spectra taken from LFEX (for shot #1) and Titan for equivalent laser intensity of $2 \times 10^{19} \text{ W/cm}^2$ is shown in Fig. 4. The positron conversion (defined as positron energy divided by the laser energy) is 3.1×10^{-5} and 1.5×10^{-4} for LFEX and Titan, respectively.

The factor of 5 difference in laser-positron conversion on LFEX and Titan appears to be correlated, on an order of magnitude scale, to the laser energy conversion of ~ 10 MeV electrons. This indicates that for the 1 mm gold target, the number of electrons with energy of about 10 MeV is important in the positron production. Note that the measured positrons that emerge from the target are a fraction of the total quantity of produced pairs. It is likely that the very high-energy electrons were not as efficient in producing pairs as the ~ 10 MeV electrons for this target thickness. This is due to a fact that the large-angle scattering of fast electrons and resulting γ -rays production become less efficient when electrons are too energetic. Optimization of target thickness for various temperature electrons has been previously studied in [36, 37].

The LFEX positron distribution was centered at ~ 12 MeV. Positron creation spectrum is typically 1-3 MeV when produced by the Beithe-Heitler processes [38]. When pulse intensity increases, we expect the peak could shift to the higher energy. In the current laser intensities the peak appears at around 5 MeV as shown in Fig. 5(a). These positron spectra are calculated from the Bremsstrahlung γ -ray spectra using the cross section of the Beithe-Heitler processes without taking into account the transport. The peak shift of the positron spectrum is explained by the sheath acceleration at the back of the target [8]. As shown in Fig. 5 (b), the PIC simulations show the onset of a sheath potential for the LFEX laser with a magnitude of 10 MV whereas the Titan a few MV. These potential agree well with the peak shift of positron spectra observed in experiments. Note here that the electron recirculation is not important in this massive gold target with 1mm thickness, where the electron takes 6 ps for one round trip. The

potential oscillation is attributed to the laser absorption processes occurred in a long scale preplasma [39].

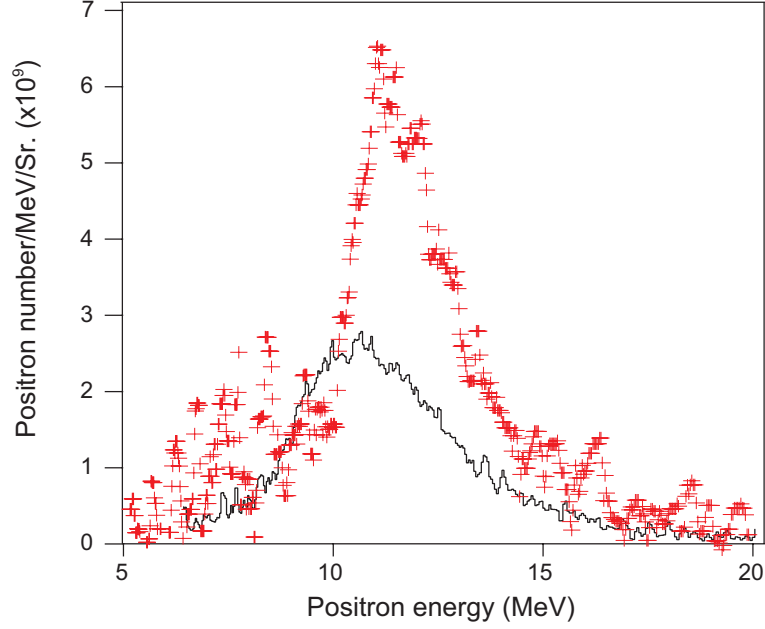


Figure 4: Positron spectra measured on LFEX (cross) and Titan (line). The laser parameters for the two shots are listed in Table 1.

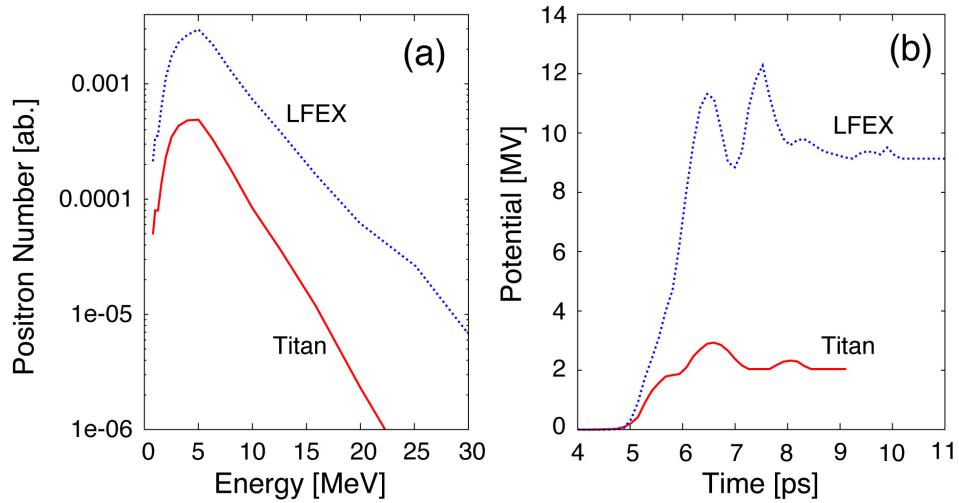


Figure 5: (a) Positron spectrum calculated from the γ -rays spectrum in PICLS simulation at the end of the simulation. (b) Time evolution of the electric potentials at the target backside in the simulations.

Summary

We reported the results of first electron-positron experiment on the LFEX laser. Measured electron spectra show that very high-energy electrons ($T_{\text{hot}} \sim 10$ MeV) were produced, indicating an intense laser pulse interacted with a long scale length pre-plasma at under-critical density. This observation was confirmed by particle-in-cell simulations. From the positron data obtained and its comparison with previous data obtained on Titan laser, we found that the ratio between laser energy to electrons at energy around 10 MeV have a large impact on positron production. In addition, our simulations show that the positron spectra peak energy location reflects closely to the sheath potentials. However, detailed quantitative correlations among the positron, bremsstrahlung and electron data are highly complex due to its large scale (mm interaction length and 10s of picoseconds interaction time). Additional large scale, multi-dimensional modeling efforts are needed to provide a more complete picture to better understand the experiment.

Acknowledgement

The authors gratefully acknowledge the support of the GEKKO XII operation group, the LFEX development and operation group and the plasma diagnostics operation group of the Institute of Laser Engineering, Osaka University. This work was performed under the auspices of the U.S. DOE by LLNL under Contract DE-AC52-07NA27344 and LDRD (#12-ERD-062), and partially funded by ILE's Joint research program.

Reference

- [1] Mike Dunne et al, "HiPER Technical Background and Conceptual Design Report 2007", June 2007; <http://www.hiperlaser.org/>
- [2] M. H. Key, Phys. Plasmas **14**, 055502 (2007).
- [3] R. Kodama, et al., Nature **412**, 798 (2001)
- [4] M. Roth, et al., Phys. Rev. Lett. **86**, 436 (2001)
- [5] R. D. Edwards, M. A. Sinclair, T. J. Goldsack, K. Krushelnick, F. N. Beg, E. L. Clark, A. E. Dangor, Z. Najmudin, M. Tatarakis, B. Walton, M. Zepf, K. W. D. Ledingham, I. Spencer, P. A. Norreys, R. J. Clarke, R. Kodama, Y. Toyama, and M. Tampo, Appl. Phys. Lett. **80**, 2129 (2002)
- [6] P. A. Norreys, M. Santala, E. Clark, M. Zepf, I. Watts, F. N. Beg, K. Krushelnick, M. Tatarakis, A. E. Dangor, X. Fang, P. Graham, T. McCanny, R. P. Singhal, W. D. Ledingham, A. Creswell, D. C. W. Sanderson, J. Magill, A. Machacek, J. S. Wark, R. Allott, B. Kennedy, and D. Neely, Phys. Plasmas **6**, 2150 (1999)
- [7] C. Courtois, A. Compant La Fontaine, O. Landoas, G. Lidove, V. Méot, P. Morel, R. Nuter, E. Lefebvre, A. Boscheron, J. Grenier, M. M. Aléonard, M. Gerbaux, F. Gobet, F. Hannachi, G. Malka, J. N. Scheurer, and M. Tarisien, PHYSICS OF PLASMAS **16**, 013105 (2009)
- [8] Hui Chen, S.C. Wilks, D.D. Meyerhofer, J. Bonlie, C.D. Chen, S.N. Chen, C. Courtois, L. Elberson, G. Gregori, W. Kruer, O. Landoas, J. Mithen, J. Myatt, C.D. Murphy, P. Nilson, D. Price, M. Schneider, R. Shepherd, C. Stoeckl, M. Tabak, R. Tommasini, P. Beiersdorfer, Phys. Rev. Lett. **105**, 015003 (2010)
- [9] Hui Chen, D. D Meyerhofer, S. C. Wilks, R. Cauble, F. Dollar, K. Falk, G. Gregori, A. Hazi, E. I. Moses, C. D. Murphy, J. Myatt, J. Park, J. Seely, R. Shepherd, A. Spitkovsky, C. Stoeckl, C. I. Szabo, R. Tommasini, C. Zulick, P. Beiersdorfer, High Energy Density Physics, **7**, 225 (2011)
- [10] K. B. Wharton, S. P. Hatchett, S. C. Wilks, M. H. Key, J. D. Moody, V. Yanovsky, A. A. Offenberger, B. A. Hammel, M. D. Perry, and C. Joshi, Physical Review Letters, **81**, 825 (1998)
- [11] F. N. Beg, A. R. Bell, A. E. Dangor, C. N. Danson, A. P. Fews, M. E. Glinsky, B. A. Hammel, P. Lee, P. A. Norreys, and M. Tatarakis, Physics of Plasmas **4**, 447, (1997).
- [12] R. B. Stephens, R. A. Snavely, Y. Aglitskiy, F. Amiranoff, C. Andersen, D. Batani, S. D. Baton, T. Cowan, R. R. Freeman, T. Hall, S. P. Hatchett, J. M. Hill, M. H. Key, J. A. King, J. A. Koch, M. Koenig, A. J. MacKinnon, K. L. Lancaster, E. Martinolli, P. Norreys, E. Perelli-Cippo, M. Rabec Le Gloahec, C. Rousseaux, J. J. Santos, and F. Scianitti, Phys. Rev. E **69**, 066414 (2004).
- [13] T. Ma, H. Sawada, P. K. Patel, C. D. Chen, L. Divol, D. P. Higginson, A. J. Kemp, M. H. Key, D. J. Larson, S. Le Pape, A. Link, A. G. MacPhee, H. S. McLean,

- Y. Ping, R. B. Stephens, S. C. Wilks, and F. N. Beg, Phys. Rev. Lett. **108**, 115004 (2012)
- [14] C. D. Chen, P. K. Patel, D. S. Hey, A. J. Mackinnon, M. H. Key, K. U. Akli, T. Bartal, F. N. Beg, S. Chawla, H. Chen, R. R. Freeman, D. P. Higginson, A. Link, T. Y. Ma, A. G. MacPhee, R. B. Stephens, L. D. Van Woerkom, B. Westover, and M. Porkolab, Phys. Plasmas **16**, 082705 (2009).
- [15] T. E. Cowan, A. W. Hunt, T. W. Phillips, S. C. Wilks, M. D. Perry, C. Brown, W. Fountain, S. Hatchett, J. Johnson, M. H. Key, T. Parnell, D. M. Pennington, R. A. Snavely, and Y. Takahashi, Phys. Rev. Lett. **84**, 903 (2000)
- [16] H. A. Bethe and W. Heitler. On the stopping of fast particles and on the creation of positive electrons. Proc. Roy. Soc. (London), **A146**, 1934.
- [17] Y. Sentoku and A. J. Kemp. J. Comp. Phys. **227**, 6846 (2008)
- [18] P. M. Nilson, A. A. Solodov, J. F. Myatt, W. Theobald, P. A. Jaanimagi, L. Gao, C. Stoeckl, R. S. Craxton, J. A. Delettrez, B. Yaakobi, J. D. Zuegel, B. E. Kruschwitz, C. Dorrer, J. H. Kelly, K. U. Akli, P. K. Patel, A. J. Mackinnon, R. Betti, T. C. Sangster, and D. D. Meyerhofer, PHYSICS OF PLASMAS **18**, 056703 (2011)
- [19] http://www.ile.osaka-u.ac.jp/zone2/collab/facilities/A/LFEX_info.htm
- [20] Z. Zhang, H. Nishimura, T. Namimoto, S. Fujioka, Y. Arikawa, M. Nishikino, T. Kawachi, A. Sagisaka, H. Hosoda, S. Orimo, K. Ogura, A. Pirozhkov, A. Yogo, Y. Okano, H. Kiriyama, K. Kondo, S. Ohshima, and H. Azechi, REVIEW OF SCIENTIFIC INSTRUMENTS **83**, 053502 (2012)
- [21] Hui Chen, A. J. Link, R. van Maren, P. K. Patel, R. Shepherd, S. C. Wilks, and P. Beiersdorfer, Review of Scientific Instruments **79**, 10E533 (2008).
- [22] http://www.bubbletech.ca/radiation_detectors_files/Bubble%20Detectors.html
- [23] J. Myatt, W. Theobald, J. A. Delettrez, C. Stoeckl, M. Storm, T. C. Sangster, A. V. Maximov, and R. W. Short, Phys. Plasmas **14**, 056301 (2007)
- [24] Zulick, F. J. Dollar, H. Chen, K. Falk, A. Hazi, C. Murphy, J. Park, J. Seely, C. I. Szabo, R. Tommasini, R. Shepherd, and K. Krushelnick, Can. J. Phys. **89**, 647 (2011)
- [25] G. J. Williams, B. R. Maddox, Hui Chen, S. Kojima, M. Millecchia, M. Rowland, C. Sorce, G. F. Stone, D. Walker, to be submitted to Rev. Sci. Instrum (2012)
- [26] Z. Zhang, H. Nishimura, T. Namimoto, S. Fujioka, Y. Arikawa, M. Nakai, T. Ozaki, M. Koga, H. Chen, J. Park, G. J. Williams, H. Shiraga, S. Kojima, M. Nishikino, T. Kawachi, A. Sagisaka, S. Orimo, K. Ogura, A. Pirozhkov, A. Yogo, Y. Okano, H. Kiriyama, K. Kondo, H. Hosoda, and H. Azechi, APS/DPP: DPP12-2012-000856 (2012)
- [27] Hui Chen et al., Phys. Rev. Lett. **102**, 105001 (2009).
- [28] L. A. Cottrill, A. Kemp, M. Tabak, and R. P. J. Town, Nucl. Fusion **50**, 095002 (2010).

- [29] A. Link, R. R. Freeman, D. W. Schumacher, and L. D. Van Woerkom, PHYSICS OF PLASMAS **18**, 053107 (2011)
- [30] S. C. Wilks, W. L. Kruer, M. Tabak, and A. B. Langdon. Absorption of ultra-intense laser pulses. Phys. Rev. Lett., 69(9):1383–1386, Aug 1992.
- [31] M. G. Haines, M. S. Wei, F. N. Beg, and R. B. Stephens, Physical Review Letters, 102(4):045008, 2009.
- [32] A. Pukhov A and J. Meyer-ter-Vehn, Phys. Plas. **6** 2847 (1999)
- [33] N. Naseri, S. G. Bochkarev and W. Rozmus, Phys. Plas. **17** 033107 (2010)
- [34] Alexey V. Arefiev, Boris N. Breizman, Marius Schollmeier, and Vladimir N. Khudik, PRL 108, 145004 (2012)
- [35] L. Willingale, P. M. Nilson, A. G. R. Thomas, S. S. Bulanov, A. Maksimchuk, W. Nazarov, T. C. Sangster, C. Stoeckl, K. Krushelnick, Phys. Plas. **18** 056706 (2011)
- [36] Alexander Henderson, Edison Liang, Pablo Yepes, Hui Chen and Scott Wilks, Astrophysics and Space Science, 295 (2011)
- [37] Yonghong Yan, Yuchi Wu, Zongqing Zhao, Jian Teng, Jinqing Yu et al. Phys. Plasmas **19**, 023114 (2012)
- [38] K. Nakashima, and H. Takabe, Phys. Plasmas **9**, 1505 (2002)
- [39] A. J. Kemp, Y. Sentoku, and M. Tabak, PRL 101, 075004 (2008)